Frequency dependence of level depletion in Na clusters and in C2H4

S Vidal, Z P Wang, P M Dinh, P.-G Reinhard, E Suraud

Frequency dependence of level depletion in Na clusters and in C_2H_4

S. Vidal[1,2], Z. P. Wang[1,2,3], P. M. Dinh[1,2], P.-G. Reinhard[4], E. Suraud[1,2]

1) Université de Toulouse; UPS; Laboratoire de Physique Théorique (IRSAMC); F-31062 Toulouse, France
2) CNRS; LPT (IRSAMC); F-31062 Toulouse, France
3) School of Science, JiangNan University, Wuxi 214122, China
4)Institut für Theoretische Physik, Universität Erlangen, D-91058 Erlangen, Germany

PACS numbers: 31.15.ee,31.70.Hq,33.80.Eh,36.40.Vz,71.15.Mb

Abstract. In the framework of time-dependent density-functional theory, we study electron emission from Na clusters and the C_2H_4 molecule as induced by irradiation with an intense pulse. The collision of a charged projectile on C_2H_4 is also explored for comparison. We look in particular at the level depletion, i.e. the electron loss in each single-electron level separately. It is found that the distribution of electron loss depends sensitively on the photon frequency. Frequencies close to visible light remove electrons exclusively from the vicinity of the Fermi surface while light in the higher UV range (up to 20 eV for Na clusters and up to 136 eV for C_2H_4) depletes all levels about equally strong, down to the deepest bound valence state.

1. Introduction

Photons have been since long a major tool for analyzing the electronic structure of molecules [1] and clusters [2, 3]. In early times, one measured mostly the excitation spectrum through photo-absorption spectrocopy. In the meantime, the enormous progress in coherent light sources and detection setups has dramatically enhanced the variety of photon experiments with molecules and clusters. We mention here briefly the violent cluster dynamics induced by high-intensity infrared laser beams leading to emission of energetic electrons, ions, X-rays and even nuclear reactions, see e.g. [4, 5, 6, 7]. Pulses in the fs range have opened a wide area of fs-spectroscopy allowing the detailed tracking of ionic dynamics in molecules and clusters, see e.g [8, 9, 10, 11]. At the side of observables, one reveals more information by analyzing with photo-electron spectroscopy energy and angular distributions of the electrons emitted from the excited molecule [12]. The experimental tools for such analysis have also much developed lately and are increasingly being used (for an overview in cluster physics, see [13]). A rather recent achievement is the availability of coherent light beyond the visible, ranging from UV up to X-rays. A particularly versatile source is here given by the free electron lasers (FEL) [14] which can be tuned to deliver fs pulses at high frequency and simultaneously high intensity. The new options have soon been exploited, see e.g. the pioneering experiment with short X-ray pulses on rare gas clusters [15], and much been used since, for a review see [16]. It is now in reach to study in all detail photo-emission from deep lying electronic states in neutral or cationic molecules and clusters. Photo-electron spectra, e.g., allow to deduce to which extent each separate electron level is depleted by the photon pulse. The distribution of electron removal is of interest as such and it has consequences for the subsequent cluster dynamics [17]. This motivates us to investigate the features of electron depletion in dependence of photon frequency. As a tool for this investigation, we employ time-dependent density functional theory (TDDFT) at the level of the local-density approximation (LDA). This is augmented by a self-interaction correction (SIC) to describe emission properties correctly. The scheme has been much used for the description of clusters dynamics in all regimes [18, 13]. We have recently extended it to the case of organic molecules [19]. In this paper, we consider as test cases cationic Na clusters and the ethylene molecule C_2H_4 irradiated by fs laser pulses in the regime of VUV-radiation and of X-ray FEL. We address the issue of ionization mechanism, that is the extraction of electrons from least bound states or from deeper levels. We scan the level depletion as a function of laser frequency and/or intensity, in order to discriminate the ionization mechanism in each case. The paper is outlined as follows: In section 2, we introduce briefly the formal and numerical scheme. In section 3, we present and discuss the results.

2. Theoretical framework

The laser induced electron dynamics is described by the time-dependent local-density approximation (TDLDA) in standard manner, for details see e.g. [18, 13]. The calculation is restricted to valence electrons. These are the $3s$ electrons in Na, the $2s$ and $2p$ electrons in C, and naturally the $1s$ electron in H. The coupling of the ionic cores to the valence electrons is described by pseudopotentials. For the C and H atoms of the ethylene molecule, we use Goedecker-type [20] pseudopotentials consisting in a local part and a non-local contribution, all of them employing Gaussians augmented by a polynomial. The original parameterizations of [20] employ different Gaussian widths for the local part and for the various non-local projectors. This is a great hindrance for computations on a coordinate space grid. Thus we have refitted the pseudopotential parameters to employ the same width of 0.412 a_0 in all terms (local and non-local) and for both elements (C and H) involved in the study, see Appendix A. Metal clusters are less demanding. Much simpler local pseudopotentials suffice. We employ here the soft Gaussian potentials as given in [21]. The elimination of core electrons through pseudopotentials requires that the laser frequencies in the study stay safely below values which could ionize core electrons. For Na, the eliminated $2p$ state lies at -28.8 eV, while the $1s$ state for C is at -270.5 eV [22]. We use at most

19.4 eV for Na clusters and 136 eV for C_2H_4 which is on the safe side in both cases.

The LDA employs the exchange-correlation energy functional from [23]. Pure LDA understimates grossly ionization potentials (IP), but correct IP are crucial for an appropriate dynamical description of electron emission. Therefore, we augment LDA by a SIC for which we employ actually the technically inexpensive average-density SIC (ADSIC) [24].

The time-dependent fields and wave functions for C_2H_4 are represented on a 3D cartesian coordinate-space grid of dimensions $72 \times 72 \times 64$. In the case of metal clusters, we use a cylindrically averaged pseudopotential scheme [25, 26]. The size of the corresponding cylindical box is for Na_9^+ 45 in radial and 91 in longitudinal directions (with a mesh size of 0.8 a_0), and for Na_{22}^{++}, 81×173 respectively. Electronic wave functions are propagated in time by the time-splitting method [27]. We use a time step of 6×10^{-4} fs for C_2H_4 and 4.8×10^{-3} fs for Na clusters. The Poisson equation is solved by a fast Fourier technique combined with separate treatment of the long-range terms [28]. We use absorbing boundary conditions at the outskirts of the grid [18, 13, 29]. This absorbs all outgoing electron flow reaching the bounds of the grid and thus prevents artefacts from reflection back into the reaction zone.

We used pulse lengths of 40 fs for C_2H_4, and 80 fs for Na clusters. We pursued the simulations further over some tens of fs, in order to complete the direct electron emission [30, 18]). Although, our dynamical propagation scheme can deal with a simultaneous propagation of ionic motion [18, 13], we kept the ions frozen in case of C_2H_4 to reduce computational expense. Ionic motion plays a minor role at the time scales studied here.

The observables discussed in this paper are electronic dipole moment and ionization $N_{\rm esc}$ (= number of escaped electrons). The dipole moment of valence electrons with respect to ions, $\mathbf{D}(t)$, is evaluated as

$$\mathbf{D}(t) = \int \mathrm{d}^3\mathbf{r}\,(\mathbf{r} - \mathbf{R}_{\rm cm,ion})\,n(\mathbf{r},t) \quad , \tag{1}$$

where $n(\mathbf{r},t) = \sum_\alpha |\varphi_\alpha(\mathbf{r}t)|^2$ is the total electronic density and the φ_α are the occupied electron wave functions. As mentioned above, absorbing boundary conditions are used to remove outgoing electrons. The absorption leads to a loss of norm of each single particle state. This, in turn, allows one to compute for each state φ_α the level depletion $\nu^{(\alpha)}$, the average ionization $N_{\rm esc}^{(\alpha)}$ out of state φ_α and also the total average ionization $N_{\rm esc}$, by

$$\nu^{(\alpha)}(t) \;= 1 - \langle\varphi_\alpha(t)|\varphi_\alpha(t)\rangle, \tag{2a}$$

$$N_{\rm esc}^{(\alpha)}(t) = n_\alpha\,\nu^{(\alpha)}(t), \tag{2b}$$

$$N_{\rm esc}(t) \;= \sum_\alpha N_{\rm esc}^{(\alpha)}(t), \tag{2c}$$

where n_α is the occupation number in state φ_α. The numerical simulations are performed over a sufficiently long time to collect all ionization, i.e. up to a point where the $\nu^{(\alpha)}(t)$ do not change anymore.

It is to be noted that these $\nu^{(\alpha)}(t)$ are averaged quantities as any observable computed as an expectation value from a mean field state. And the total $N_{\rm esc}$ yields the average number of emitted electrons, representing a large ensemble of measurements. One may use these numbers to recover detailed ionization probabilities for each charge state (for details see, e.g., [18, 13]). The present discussion is confined to average ionizations which already carry a great deal of information.

3. Results and discussion

In all cases considered here, the laser intensity has been adjusted so that the total ionization remains small. This means that all results stay in a perturbative regime where response amplitudes and emission yields scale with the total number of emitted electrons $N_{\rm esc}$, or intensity I respectively. We will inspect in the following the "relative level depletion" $\nu^{(\alpha)}/N_{\rm esc}$ which are in the perturbative regime independent of laser intensity or total yield.

3.1. Na clusters

We start with the case of Na clusters and first discuss Na_9^+. This cluster has three distinctive valence electron energy levels : the $1s$ level (filled with 2 valence electrons) at -8.6 eV, the $1p_z$ level (with 2 electrons) at -7.4 eV, and the HOMO, nearly degenerated, $1p_{x,y}$ levels (with 4 electrons in total) at -7.2 eV, which also gives the IP. As all metal clusters, the cluster shows a pronounced Mie plasmon resonance which comes here at around 2.5 eV [2, 3]. This cluster is irradiated with a laser pulse of total length of 80 fs and at various frequencies, ranging from 6.8 to 20.4 eV. All frequencies are far above the Mie plasmon resonance. The lowest frequency is below the IP, while the others are sufficiently large to ionize all valence levels in a one-photon process.

One may suspect that the perturbation by the external laser field spoils the levels which we want to explore. This effect was studied for Na clusters in [31] and it was found that the amount of perturbation depends on the strength of the external field. The effect can be quantified in terms of the average number of emitted electrons. Strong perturbations are associated with about one or more emitted electrons. Staying at emission yields of a few percent means to deal with small perturbations where the electronic structure, in particular the single-particle energies, remains basically unchanged. We have taken care to tune the laser intensities properly to guarantee that one resides always in the regime of weak perturbation, see below. We have checked that the single-particle energies indeed remain well defined and quasi constant in time. To demonstrate the relevance of the emission data, we show in Fig. 1 two computed photo-electron spectra (PES) for Na_9^+ irradiated by lasers whose frequencies lie in the UV domain. The PES exhibit typical couples of peaks corresponding to the $1s$ and the $1p$ states of Na_9^+. More precisely, the peaks exactly lie at an electron kinetic energy given by $\varepsilon_{\rm kin} = \varepsilon_i + n\,\hbar\omega_{\rm las}$ where ε_i denotes the energy of state i and n the number of photons involved in the process. For $\omega_{\rm las} = 6.8$ eV, one can spot 2-, 3- and 4-photon processes, while for the higher frequency, 1, 2 and 3 photons are involved. Moreover, in the low ionization regime, the peaks turn out to be extremely narrow. This clearly indicates that, over the whole dynamical process, the associated single particle energies have not been modified [31]. The sharpness of the peaks furthermore ensures that they remain well separated in energy. This figure thus demonstrates that, as soon as the total ionization remains small (in this case here, less than 0.01), no state mixing occurs and the single particle energies of the ground state can be tracked and studied within our dynamical calculations.

We now discuss more specifically the level depletion. The intensity I of the laser pulse was varied to track its effect on the detailed depletion pattern. We found that relative depletion is insensitive to intensity as long as one stays in a (perturbative) regime of low emission (less than 0.1 electron). Nonetheless, we tune the intensity to frequency such that the net yield remains roughly comparable over all frequencies in a given case. This means, e.g., that we use $I = 9 \times 10^{12}$ W/cm^2 for $\omega_{\rm las} = 6.8$ eV, 9×10^{13} W/cm^2 for $\omega_{\rm las}$ between 10.9 and 15.0 eV, and 5×10^{14} W/cm^2 for $\omega_{\rm las} = 19.4$ and 20.4 eV. Fig. 2 shows the relative ionizations and depletions as a function of $\omega_{\rm las}$. According to the top panel, the ionization yield is dominated by the $1p_{xy}$ states, while the $1p_z$ and the $1s$ states change relative importance with a crossing between, around 13.2 eV. Both ionizations from the latter levels stay below that from the $1p_{xy}$

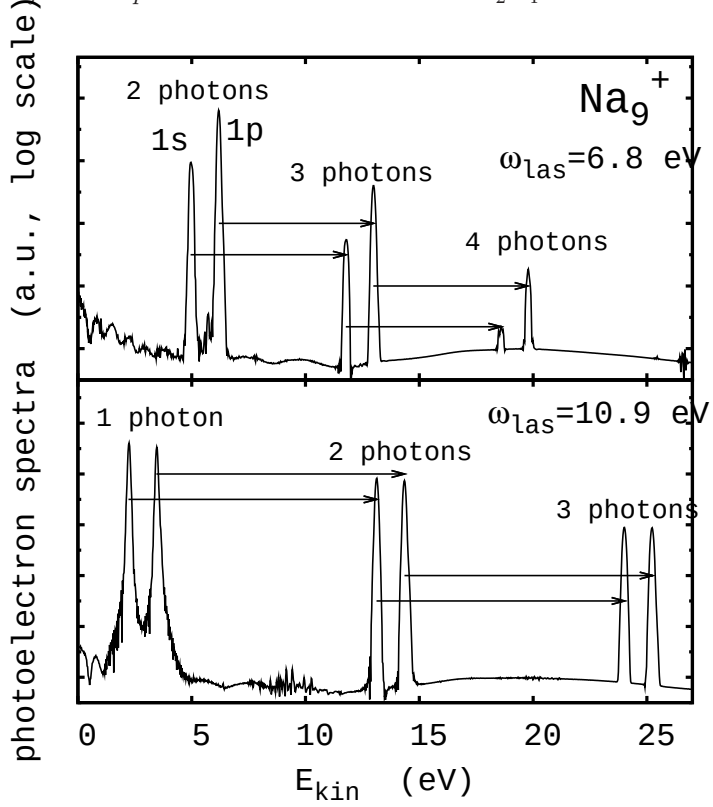

Figure 1. Calculated photoelectron spectra of Na_9^+ irradiated with a laser pulse of pulse length 80 fs and for two laser frequencies ω_{las}. The laser intensities are $I = 2\times10^{11}$ W/cm^2 and $I = 2\times10^{12}$ W/cm^2 for the top and the bottom panels respectively. The arrows indicate the shift value between the peaks and match the value of the laser frequency.

states. Note, however, that the $N_{esc}^{(\alpha)}/N_{esc}$ is weighted by the multiplicity of state α, see Eq. (2b), and that there are 4 electrons in the $1p_{xy}$ states, while the $1s$ and the $1p_z$ states have 2 electrons each. This causes the dominance of emission from $1p_{xy}$.

Probably a better comparison of ionization mechanisms is achieved by plotting the relative level depletion $\nu^{(\alpha)}/N_{esc}$, Eq. (2a), instead of the relative level ionization $N_{esc}^{(\alpha)}/N_{esc}$. This is done in the bottom panel of Fig. 2. For the lowest frequency, ionization still comes dominantly from the HOMO ($1p_{xy}$), but now close up with the nearly degenerate $1p_z$, while the $1s$ state contributes very little, almost one order of magnitude less. Increasing the frequency does not modify so much the depletion from the $1p_{xy}$ states. But the depletion of the $1s$ state is almost steadily increasing while the $1p_z$ state falls below the other states for the higher frequencies. All three states have almost equal depletion around 13 eV. Above 14 eV, the contribution from the $1p_z$ steadily decreases, while that from the $1s$ level becomes more and more dominant. The trends of the level depletion show some fluctuations indicating some oscillatory behaviour of the level depletion at a fine energy scale. This point will be addressed in more detail in Fig. 4.

The results on Na_9^+ indicate that low frequency laser pulses remove electrons preferentially from the Fermi surface while high frequency pulses extract electrons more equidistributed, even with a preference for the most bound state. We check that such depletion patterns are not accidental by investigating the case of Na_{22}^{++}. Fig. 3 presents the depletion in relation to the s.p. energies. Three cases are compared: 6.8, 10.9, and 15.0 eV. The pulse length is again 80 fs. Intensities have been adjusted in order to get in

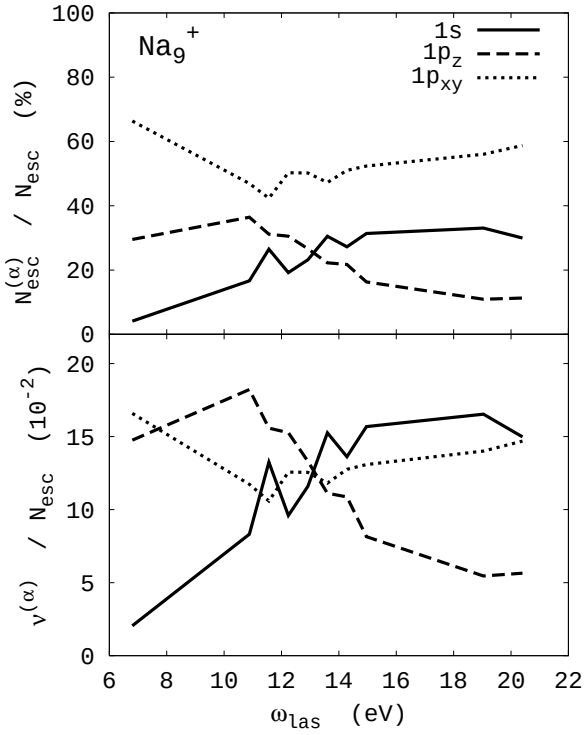

Figure 2. Relative level ionization $N_{\rm esc}^{(\alpha)}/N_{\rm esc}$ (top) and relative level depletion $\nu^{(\alpha)}/N_{\rm esc}$ (bottom), in irradiated Na_9^+ for $\alpha = 1s$, $1p_z$ and $1p_{xy}$, as a function of the laser frequency $\omega_{\rm las}$. The total pulse length is 80 fs.

all cases $N_{\rm esc} \sim 0.05$, so that the perturbative picture of constant s.p. energies in time remains valid in all cases. The features are much the same as in Na_9^+: for low frequencies, emission mainly comes from the HOMO whereas increasing frequency puts increasing weight on the more deeply bound states.

It is to be noted that the above statement holds for the general trends. The distribution of depletions can vary very much in detail because the emission strength depends on the spatial matrix element between bound single particle wave function and emitted continuum wave [32, 33]. And the latter can depend sensitively on the outgoing wave number. This detailed sensitivity to photon frequency is demonstrated in Fig. 4 showing the depletion of each occupied single electron state in Na_{22}^{++} as a function of photon frequency in a small window above 15 eV. The depletion can vary on a rather short frequency scale (see the deepest bound level at -10.14 eV) and there are also long range trends (see, e.g., the states at -9.25 eV and -8.04 eV) which may substantially change the relative distribution of level depletion for much different frequencies. The example shows that the detailed patterns of depletion are fluctuating. They require more systematic investigations and may, in turn, reveal more information on the spatial structure of the occupied states [34, 33]. We will address this issue in more detail for the case of ethylene (see discussion in Sec. 3.2.3). Above all these details remains one robust effect, namely that photon frequencies below the IP deplete preferably level near the Fermi surface while frequencies which are large enough to emit the deepest bound state at once produce more equilibrated depletion from all occcupied levels.

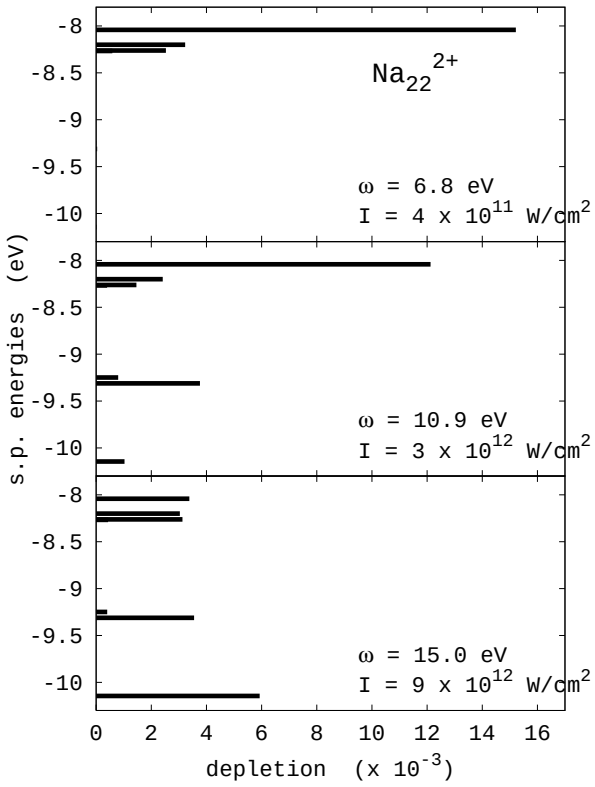

Figure 3. Depletion of single particle levels, $\nu^{(\alpha)}$, in $Na_{22}{}^{2+}$ for three laser frequencies $\omega_{\rm las}$ and intensities I as indicated. The depletion is represented by the length of the horizontal bars while the position at the y-axis indicates the energy of the corresponding level.

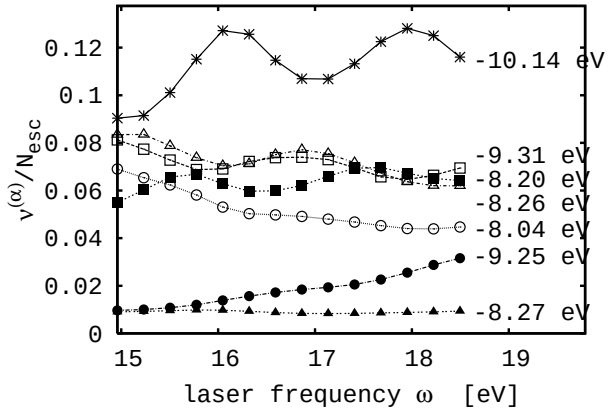

Figure 4. Relative depletion of single particle levels in $Na_{22}{}^{++}$ for a laser pulse with total length of 96 fs and intensity $I = 10^{13}$ W/cm^2. Results are drawn as a function of laser frequency. The level energy is indicated at the right side of the curves.

3.2. The ethylene molecule

We now turn to the case of an organic molecule, C_2H_4, which will allow us to explore an even larger range of laser frequencies.

3.2.1. Optical spectrum Before looking at the electronic response of this molecule after laser irradiation, we first present its optical response in Fig. 5, since the latter will help us in the choice of $\omega_{\rm las}$. The optical

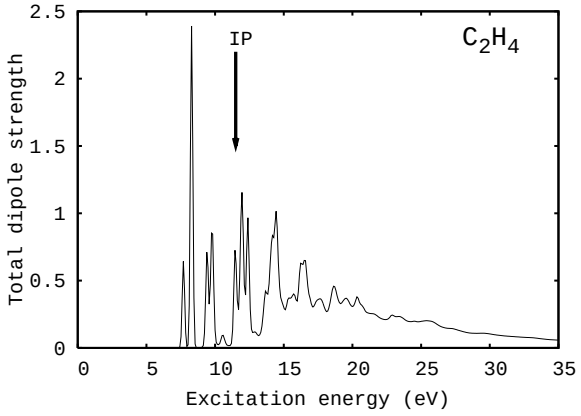

Figure 5. Total photo-absorption strength of C_2H_4. The vertical arrow corresponds to the value of the ionization potential of the molecule.

asborbing strength is deduced from the time evolution of the electronic dipole moment, defined in Eq. (1), by means of spectral analysis [35, 36, 37]. In Fig. 5, it is averaged over the three spatial directions and it is not energy weighted. It shows strong, isolated peaks at lower energies and changes to a continuum above the IP (11.5 eV). This result is consistent with former TDLDA calculations [38]. The lowest peak is at 7.74 eV, in good agreement with previous CI calculations (7.76 eV [39]). We obtain the highest peak in the optical response lying at 8.16 eV. The frequency selective laser pulses will be sensitive to this much fluctuating spectrum while a collision with fast ions will deliver a broad spectrum of frequencies and will excite all modes at once.

3.2.2. Irradiation by laser pulses We now turn to the irradiation of C_2H_4 by a laser pulse of intensity $I = 10^{13}$ W/cm^2, total pulse length of 40 fs and polarization parallel to the C-C bond. Three typical frequencies $\omega_{\rm las}$ are used : below the resonant region (6.8 eV), within that region (8.16 eV) and well above (136 eV), see Fig. 5. The six occupied valence levels are successively $(2a_g)^2$, $(2b_{1u})^2$, $(1b_{2u})^2$, $(3a_g)^2$, $(1b_{3g})^2$, and $(1b_{3u})^2$, with energies of -11.5, -12.4, -14.4, -16.0, -18.2, and -23.4 eV respectively. They are represented in real space in Fig. 6. One can notice that the states $(2a_g)$, $(2b_{1u})$ and $(3a_g)$ exhibit nodes along the C-C bond, which corresponds to the laser polarization. We also checked that no state mixing occurs in the regime of low total ionization that we explored here, as has been illustrated by the calculations of photoelectron spectra for Na_9^+, see Fig. 1.

Fig. 7 presents the time evolution of $N_{\rm esc}$ and of the dipole moment $D(t)$ along the laser polarization direction. It is obvious that both observables depend sensitively on $\omega_{\rm las}$. The left panels show the case $\omega_{\rm las} = 6.8$ eV, i.e. below the resonant region. The electronic dipole follows nicely the envelope of the laser pulse and electronic excitation fades away as soon as the laser is switched off. Electron emission is directly connected to the dipole amplitude and thus it has a maximum when the laser pulse is at its

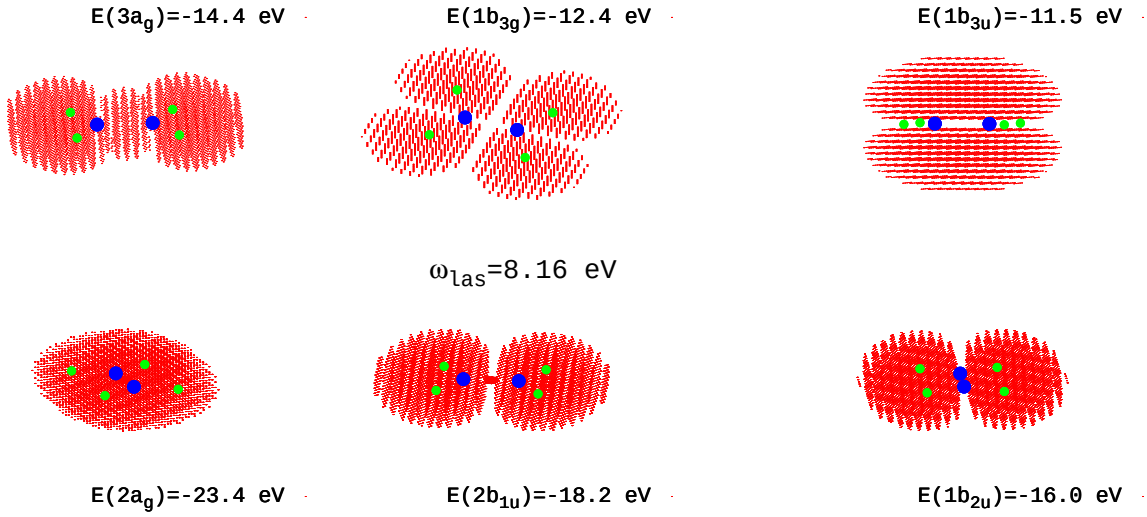

Figure 6. Electronic wave functions of the ground state of C_2H_4 represented in real space. The blue balls indicate the location of the C atoms, while the H atoms are represented by green circles. Note that the spatial orientation is different for each orbital, such that the nodes are clearly visible. The polarization of the laser we used is along the C-C bond.

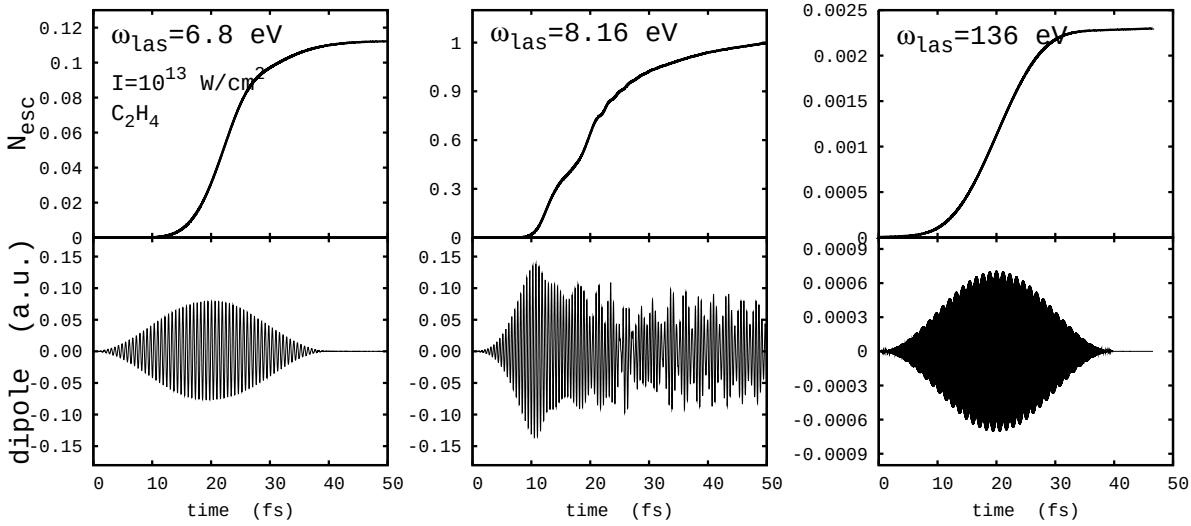

Figure 7. Time evolution of the number of escaped electrons (top panels) and the dipole moment along the laser polarization direction (bottom panels) of C_2H_4 irradiated with a laser of intensity of 10^{13} W/cm^2, pulse length of 40 fs, and for three frequencies as indicated.

maximum of amplitude. The total ionization remains small in this case (about 0.11 charge units). This pattern is very similar to what is observed in metal clusters when irradiated by an optical laser with frequency off the plasmon resonance [30].

For a laser frequency highly above the resonant region (right panels), that is here $\omega_{\rm las} = 136$ eV, we meet again an off-resonant process and the patterns look much similar. However, the net ionization is

48 times smaller compared with the low-frequency case. The suppression of emission is due to the fact that the laser field oscillates so fast that a large fraction of electronic density is kicked back before it can gain substantial velocity to escape. This strong suppression of frequency is well accounted for in the Keldysh parameter describing an effective laser strength [40]. One would have to increase the raw laser intensity I significantly in order to get ionization similar to the low-frequency case. At the side of the dipole moment, we also see a much smaller amplitude. Note some small and fast oscillations on top of the dipole profile. This stems from a (reduced) quiver motion.

The middle panels correspond to the case $\omega_{\rm las} = 8.16$ eV, which is in resonance with the strongest peak in the optical response of C_2H_4 [41]. Now the dipole signal and $N_{\rm esc}$ show the typical resonant patterns which differ from the off-resonant cases. During the first 10 fs, the dipole moment still follows the envelope of the laser pulse as in the other cases. But the resonant coupling yields a much larger amplitude. As a consequence, ionization is much larger and comes up earlier. This causes a sudden reduction of the dipole oscillations. There is again a small increase of the oscillations at around 16 fs because the now charged system drives the next peak in the optical response into resonance with the laser. The amplitude of dipole moment is attenuated again due to damping by ongoing electron emission. The attenuation is small and the dipole signal continues to oscillate on its own long after the photon pulse is switched off. Correspondingly, ionization is carrying on. It can take several ps until emission has damped the dipole signal sufficiently to terminate the growth in ionization.

3.2.3. Irradiation by a charged projectile Having sorted out the dynamical regimes, we now consider the photon induced electron emission for C_2H_4. Two photon frequencies are considered, $\omega_{\rm las} = 6.8$ eV and $\omega_{\rm las} = 136$ eV, both being off-resonant. The pulse length is 40 fs to stay in a time domain where ionic motion plays no role. This leaves the electronic ground state structure the reference point throughout the whole dynamics. Additionally, we consider the case of a collision with a singly charged projectile passing by at a distance of 9 a_0 with a velocity of $v = 20$ a_0/fs. Photon intensity and parameters of the projectile are tuned to obtain comparable total ionization $N_{\rm esc}$. Fig. 8 shows the results for the final depletion. The patterns are very similar to the previous test case Na_{22}^{++}: At low frequency, we see electron emission preferably from the HOMO and the states next to it while the high frequency (all valence levels in reach of a one-photon process) produces comparable depletion for all levels down to the deepest bound one. We now relate more precisely the level depletion to the orbital shapes (see Fig. 6), keeping in mind that the laser polarization is along the C-C bond. With $\omega_{\rm las} = 6.8$ eV, the dominant effect is an energetic one (middle panel of Fig. 8). Indeed, although the HOMO ($1b_{3u}$) has nodes along the C-C axis (visible in Fig. 6, top right), it is depleted the most because it is bound by almost 1 eV less than the HOMO-1. And comparing the depletion of the HOMO-1 and HOMO-2, the orientation of the orbitals with respect to the laser polarization now competes with the energetics : these states are separated by 2 eV but exhibit similar depletions, even higher for the HOMO-2, because it has no nodes along the C-C direction, and this is not the case for the HOMO-1 (see first row of Fig. 6). This balance between orbital energy and orbital shape is all the more predominant for the high frequency case. The least depleted states are the ($2b_{1u}$) and ($3a_g$) which have nodes along the C-C axis. It is also the case for the HOMO ($1b_{3u}$) but here, the energetics takes the lead.

The collision by a charged projectile delivers a very short Coulomb pulse to the molecule site and thus contains a broad distribution of frequencies ω which has a maximum at low ω and decays slowly with increasing ω. The depletion patterns are thus somewhat similar to the low-frequency laser case. The moderate admixture of higher frequencies allows more depletion for slightly deeper levels. There is even a small amount of emission from the deepest level. But the content of high frequency in the Coulomb pulse is obvisouly rather small. The high-frequency part could be enhanced by going to faster collisions. This, on the other hand, reduces the total emission cross section and complicates experimental detection. It is obvious that the extremely versatile (X)FEL pulses which can be tuned in pulse length, intensity, and frequency are much superior here for experimental analysis of molecular and cluster structure.

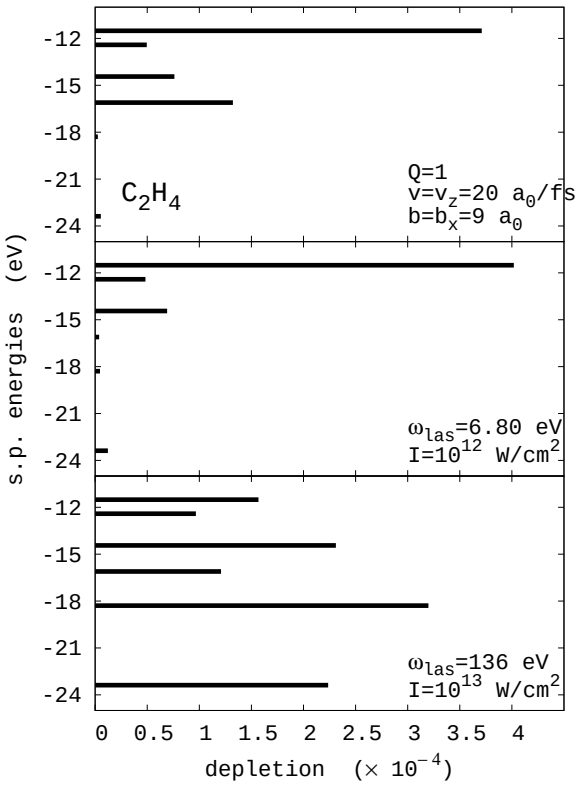

Figure 8. Level depletion for C_2H_4 irradiated by a photon pulse (bottom and middle) or by a charged projectile (top), with respective parameters as indicated. Final depletions are represented by the length of the horizontal bars while the position at the y-axis indicates the energy of the corresponding level.

4. Conclusions

In this paper, we have investigated the electronic excitation of ethylene and small sodium clusters subjected to moderate external electromagnetic fields (femtosecond photon pulses or collision with a charged projectile) applying a time-dependent density-functional approach. We have analyzed the electronic dipole moments and the number of escaped electrons for C_2H_4. When the photon frequency is off-resonant or highly above the resonant region, the dipole signal behaves as a classical oscillator in both situations and the electron emission is rather small. In contrast, for resonant frequencies, there is a substancial electronic emission and a strong damping of the dipole moments.

We have also studied in detail the level depletion of C_2H_4, Na_9^+ and Na_{22}^{2+}. For C_2H_4, the level depletion caused by a photon field or by a collision with a fast charged projectile are considered. Both for the organic molecule C_2H_4 and for small sodium clusters, a low frequency photon pulse tends to remove electrons from the surface, that is from least bound states, whereas FEL frequency pulses can extract electrons from deeper bound levels. Furthermore, we find that the level depletion pattern of C_2H_4 impacting with a fast projectile is similar to that of a low photon frequency, as long as total ionizations in both situations are comparable.

ACKNOWLEDGEMENTS

This work was supported by the National Natural Science Foundation of China (Grants No. 10575012 and No. 10435020), the National Basic Research Program of China (Grant No. 2010CB832903), the Doctoral Station Foundation of Ministry of Education of China (Grant No. 200800270017), the scholarship program of China Scholarship Council and the French Agence Nationale pour la Recherche (ANR-06-BLAN-0319-02). Calculations have been performed on the French computational facilities CalMiP, CINES, IDRIS and CCRT.

Appendix A. The non-local pseudopotential for C and H atoms

The form of the Goedecker pseudopotentials at the level of refinement as we use it here is given by [20]

$$\begin{aligned} V_{\mathrm{PsP}}(r)\,\varphi_\alpha(r) &= V_{\mathrm{loc}}(r)\,\varphi_\alpha(r) \\ &\quad + \int \mathrm{d}r'\, V_{\mathrm{nloc}}(r,r')\,\varphi_\alpha(r') \quad , \\ V_{\mathrm{loc}}(r) &= -\frac{Z_I}{r}\,\mathrm{erf}\left(\frac{r}{\sqrt{2}r_{\mathrm{loc}}}\right) \\ &\quad + C_1 \exp\left(-\frac{r^2}{2r_{\mathrm{loc}}^2}\right) \quad , \\ V_{\mathrm{nloc}}(r,r') &= p(r) h_0 p(r') \quad , \\ p(r) &= \frac{\sqrt{2}}{r_{\mathrm{nloc}}^{3/2}\sqrt{\Gamma(3/2)}} \exp\left(-\frac{r^2}{2r_{\mathrm{nloc}}^2}\right) \quad . \end{aligned}$$

where Z_I is the charge of ion, erf is the error function, and $p(r)$ is a radial projector in the separable non-local term. The original parameterizations employ different r_{loc} and r_{nloc} for each material which slows down computations. We have developed parameterizations with the same width in all terms. These pseudopotential parameters are given in Table A1. Further details will be given in a forthcoming publication.

	r_{loc} [a_0]	Z_I	C_1 [Ha]	r_{nloc} [a_0]	h_0 [Ha]
H	0.35	1	−1.75		
C	0.35	4	−4.467183	0.35	5.87018

Table A1. Parameters of the local and non-local pseudopotentials as used here for the H and C atoms.

[1] M Weissbluth. Atoms and Molecules. Academic Press, San Diego, 1978.
[2] U Kreibig and M Vollmer. Optical Properties of Metal Clusters, volume 25. Springer Series in Materials Science, 1993.
[3] H Haberland, editor. Clusters of Atoms and Molecules 1- Theory, Experiment, and Clusters of Atoms, volume 52. Springer Series in Chemical Physics, Berlin, 1994.
[4] A. McPherson, B. D. Thompson, A. B. Borisov, K. Boyer, and C. K. Rhodes. Multiphoton-induced x-ray emission at 4-5 keV from Xe atoms with multiple core vacancies. Nature, 370:631, 1994.
[5] E. Springate, S. A. Aseyev, S. Zamith, and M. J. J. Vrakking. Electron kinetic energy measurements from laser irradiation of clusters. Phys. Rev. A, 68(5):053201, Nov 2003.
[6] J. Zweiback, T. E. Cowan, J. H. Hartley, R. Howell, K. B. Wharton, J. K. Crane, V. P. Yanovsky, G. Hays, R. A. Smith, and T. Ditmire. Detailed study of nuclear fusion from femtosecond laser-driven explosions of deuterium clusters. Phys. Plasmas, 9(7):3108–3120, 2002.
[7] U. Saalmann, C. Siedschlag, and J. M. Rost. Mechanisms of cluster ionization in strong laser pulses. J. Phys. B, 39, February 2006.

[8] A. H. Zewail. Femtochemistry : Atomic-Scale Dynamics of the Chemical Bond. J. Phys. Chem. A, 104(24):5660–5694, May 2000.

[9] J. H. Posthumus. The dynamics of small molecules in intense laser fields. Rep. Prog. Phys., 67(5):623, 2004.

[10] R. E. Carley, E. Heesel, and H. Fielding. Femtosecond lasers in gas phase chemistry. Chem. Soc. Rev., 34:949–969, 2005.

[11] I. V. Hertel and W. Radloff. Ultrafast dynamics in isolated molecules and molecular clusters. Rep. Prog. Phys., 69(6):1897, 2006.

[12] J Berkowitz. Photoabsorption, Photoionization and Photoelectron Spectroscopy. Academic Press, New York, 1979.

[13] P-G Reinhard and E Suraud. Introduction to Cluster Dynamics. Wiley, New York, 2003.

[14] C Brau. Free-electron lasers. Academic Press, New York, 1990.

[15] H. Wabnitz, L. Bittner, A. R. B. de Castro, R. Döhrmann, P. Gürtler, T. Laarmann, W. Laasch, J. Schulz, A. Swiderski, K. von Haeften, T. Möller, B. Faatz, A. Fateev, J. Feldhaus, C. Gerth, U. Hahn, E. Saldin, E. Schneidmiller, K. Sytchev, K. Tiedtke, R. Treusch, and M. Yurkov. Multiple ionization of atom clusters by intense soft X-rays from a free-electron laser. Nature, 420:482–485, December 2002.

[16] T. Pfeifer, C. Spielmann, and G. Gerber. Femtosecond x-ray science. Rep. Prog. Phys., 69(2):443, 2006.

[17] F. Calvayrac, P.-G. Reinhard, and E. Suraud. Coulomb explosion of a Na_{12} cluster in a diabatic electron–ion dynamical picture. J. Phys. B, 31:5023, 1998.

[18] F Calvayrac, P-G Reinhard, E Suraud, and C A Ullrich. Nonlinear electron dynamics in metal clusters. Phys. Rep., 337:493, 2000.

[19] Z. P. Wang, P. M. Dinh, P.-G. Reinhard, E. Suraud, G. Bruny, C. Montano, S. Feil, S. Eden, H. Abdoul-Carime, B. Farizon, M. Farizon, S. Ouaskit, and T. D. Maerk. Microscopic studies of atom-water collisions. Intern. J. Mass Spectr., 285(3):143, 2009.

[20] S Goedecker, M Teter, and J Hutter. Separable dual-space gaussian pseudopotentials. Phys. Rev. B, 54:1703, 1996.

[21] S Kümmel, M Brack, and P-G Reinhard. Ionic geometries and electronic excitations of na_9^+ and na_{55}^+. Eur. Phys. J. D, 9:149, 1999.

[22] `http://physics.nist.gov/PhysRefData/DFTdata/Tables/ptable.html`.

[23] J P Perdew and Y Wang. Accurate and simple analytic representation of the electron-gas correlation energy. Phys. Rev. B, 45:13244, 1992.

[24] C Legrand, E Suraud, and P-G Reinhard. Comparison of self-interaction-corrections for metal clusters. J. Phys. B, 35:1115, 2002.

[25] B Montag and P-G Reinhard. Small metal clusters in a cylindrically averaged pseudopotential scheme. Phys. Lett. A, 193:380, 1994.

[26] B Montag and P-G Reinhard. Ionic structure and global deformation of axially symmetric simple metal clusters. Z. f. Physik D, 33:265, 1995.

[27] M D Feit, J A Fleck, and A Steiger. Solution of the schrdinger equation by a spectral method. J. Comp. Phys., 47:412, 1982.

[28] G Lauritsch and P-G Reinhard. An fft solver for the coulomb problem. Int. J. Mod. Phys. C, 5:65, 1994.

[29] P.-G. Reinhard, P. D. Stevenson, D. Almehed, J. A. Maruhn, and M. R. Strayer. Role of boundary conditions in dynamic studies of nuclear giant resonances. Phys. Rev. E, 73:036709, 2006.

[30] P-G Reinhard, F Calvayrac, C Kohl, S Kümmel, E Suraud, C A Ullrich, and M Brack. Frequencies, times, and forces in the dynamics of na clusters. Eur. Phys. J. D, 9:111, 1999.

[31] A Pohl, P-G Reinhard, and E Suraud. Towards single particle spectroscopy of small metal clusters. Phys. Rev. Lett., 84:5090, 2000.

[32] F H M Faisal. Theory of Multiphoton Processes. Plenum Press, New York, 1987.

[33] A Pohl, P-G Reinhard, and E Suraud. Angular distribution of electrons emitted from na clusters. Phys. Rev. A, 70:023202, 2004.

[34] O Frank and J Rost. Diffraction effects in the photoionization of clusters. Chem. Phys. Lett., 271:367, 1997.

[35] F Calvayrac, P-G Reinhard, and E Suraud. Non linear plasmon response in highly excited metallic clusters. Phys. Rev. B, 52:R17056, 1995.

[36] K Yabana and G F Bertsch. Phys. Rev. B, 54:4484, 1996.

[37] F Calvayrac, P-G Reinhard, and E Suraud. Spectral signals from electronic dynamics in sodium clusters. Ann. Phys. (NY), 255:125, 1997.

[38] T. Nakatsukasa and K. Yabana. Photoabsorption spectra in the continuum of molecules and atomic clusters. J. Chem. Phys., 114:2550, 2001.

[39] C. Petrongolo, R. J. Buenker, and S. D. Peyerimhoff. Nonadiabatic treatment of the intensity distribution in the v-n bands of ethylene. J. Chem. Phys., 76:3655, 1982.

[40] L V Keldysh. Sov. Phys. JETP, 20:1307, 1964.

[41] Z. P. Wang, P. M. Dinh, P.-G. Reinhard, E. Suraud, and F. S. Zhang. Nonadiabatic effects in the irradiation of ethylene. Intern. J. Quant. Chem., 2010. in press.